JOURNAL OF MATERIALS SCIENCE 31 (1996) 5897–5905

Transverse properties of a Ti–6–4 matrix/SiC fibre-reinforced composite under monotonic and cyclic loading

P. J. COTTERILL, P. BOWEN
IRC in Materials for High Performance Applications/School of Metallurgy and Materials, The University of Birmingham, Edgbaston, Birmingham B15 2TT, UK

The transverse response of a Ti–6–4/SM1140+ fibre-reinforced composite to both monotonic and cyclic loading has been investigated. Five distinct regions were found in the monotonic stress versus strain curve: (I) elastic deformation of the composite, (II) failure of the fibre/matrix interfaces, (III) elastic deformation of the remaining matrix ligaments, (IV) yielding of the matrix ligaments, and (V) gross plastic deformation, which ultimately leads to specimen failure. The stresses at which interface debonding, matrix yield and final failure occurred rose with increased displacement rate. Stressing to levels above the interface failure stress caused significant damage and limited ($\approx$0.025%) plastic deformation. A non-linear stress–strain response was observed on unloading/reloading, because the presence within the specimen of constrained "holes" (containing debonded fibres) resulted in non-homogeneous elastic straining of the matrix. The transverse low-cycle fatigue lives of Ti–6–4/SM1140+composite specimens were strongly dependent on maximum stress for values up to the interfacial failure stress, but less so for maximum stresses greater than 260–265 MPa, where full fibre/matrix debonding had occurred. Fatigue life was also dependent on the uniformity of fibre spacings within the composite.

1. Introduction

In recent years there has been extensive research designed to characterize fully the properties of titanium matrix composites reinforced with continuous ceramic fibres. The major advantages that these materials offer are their high strength- and stiffness-to-weight ratios. These properties are particularly important for aerospace applications where the use of such composites could allow significant weight savings compared to components manufactured from conventional high-temperature monolithic alloys.

The majority of the work on unidirectionally reinforced composites has thus far concentrated on their response to longitudinal stresses [1–8], which will be the primary loading direction in service. However, it has become clear that transverse stresses are present in cracked components, even when they are subjected to longitudinal loading [9]. It is therefore also important that the response of such composites to transverse stresses is established.

The material studied here was a Ti–6Al–4V matrix composite reinforced with either 31% or 33% volume fraction of SM1140+ carbon-coated silicon carbide fibres (diameter $\approx$100 μm). The first stage of the project involved a series of monotonic tensile tests designed to (i) characterize the stress versus strain response, (ii) ascertain any effect of varying the displacement rate, and (iii) determine the effect of unloading and reloading. The work then progressed on to the measurement of low-cycle fatigue life as a function of maximum stress, and the results of this study have been related to the measured tensile properties. There is also a discussion of systematic variations in the properties measured from specimens cut both from different plates, and also from different regions of the same plate.

2. Experimental procedure

The Ti–6–4/SM1140+composite material was received in the form of two 8-ply plates of thicknesses $\approx$1.40 mm (plate I) and 1.35 mm (plate II) and with fibre volume fractions $\approx$31% and 33%, respectively. These plates were machined using electro-discharge machining (EDM) to produce testpieces of length 200 mm and width 4 mm, such that the specimen length was perpendicular to the direction of reinforcement. The specimens were tested in their as-machined condition, and were given no subsequent heat treatments or surface modifications.

All tests were conducted on a 100 kN Instron 1273 servo-hydraulic testing machine, controlled through an 8500 console. The testpieces were gripped hydraulically at each end between serrated plates which exerted a pressure of approximately 20 MPa. The effective gauge length of the specimen (i.e. the distance

0022–2461

between the grips) was 70 mm, and during monotonic tensile testing the strain in the middle 50 mm of the specimen was monitored using an extensometer. Prior to each test, an acoustic emission sensor was affixed (using a cyanoacrylate adhesive) to an unstressed end of the specimen where it protruded beyond the lower grip plates.

All monotonic tensile tests were carried out under position control, and at ramp rates varying from 1–10 000 $\mu m\,min^{-1}$. A load versus extension trace was recorded on an X–Y chart recorder, and the maximum load attained was also recorded by the Instron control console. Stress versus strain curves were constructed in each case, allowing the measurement of various gradients, stresses and strains. Further details concerning these measurements are given in Section 3.

The S–N fatigue loading was carried out under load control using a trapezoidal waveform of frequency = 0.25 Hz, and a load ratio of $R = 0.1$. The trapezoidal waveform started at minimum load, and consisted of four 1 s segments: (i) a ramp to maximum load, (ii) a dwell at maximum load, (iii) a ramp down to minimum load, and (iv) a dwell at minimum load. The number of cycles to specimen failure was recorded in each case.

Additional information concerning the processes occurring during monotonic and fatigue loading was obtained from an analysis of the acoustic emissions (AE) emanating from the specimens. These were detected by a PAC NANO-30 ceramic sensor, which relayed them through a 40 dB gain pre-amplifier to a LOCAN 320 data collection and analysis unit (20 dB internal gain, 50 or 60 dB threshold). Each event was recorded with its measured/calculated characteristics, the most useful of which for the current work were time of occurrence, specimen load, energy of event and amplitude of event.

3. Results

3.1. Monotonic tensile properties

A typical transverse tensile stress versus strain relationship is shown in Fig. 1, which also shows the amplitude and number of acoustic emissions recorded within discrete stress bands throughout the test. There are five distinct regions to the curve: (I) an initial linear portion, representing elastic deformation of the composite, (II) a non-linear portion, (III) a second linear region, (IV) a second deviation from linearity, and (V) a non-linear region of plastic deformation, which ultimately leads to specimen failure.

The acoustic emission data (Fig. 1a and b) show that the majority of events have amplitudes of between 60 and 75 dB, and occur during region II of the curve, suggesting that this deviation from the linear results from the brittle failure of the fibre/matrix interfaces. The second linear region III would therefore, by deduction, represent the elastic deformation of the matrix ligaments remaining between the debonded fibres, which then yield in region IV of the curve, resulting in a second deviation from linearity. From such traces, it was possible to measure a number of different properties, and these are listed in Table I. The measurement of properties was standardized through the use of computer-generated fit plots, for which a best linear fit line was constructed, giving values for the gradients of the first and second linear regions. Offset lines were then constructed with the same gradient, but with an offset of 0.005% strain, and the points of deviation from the linear were taken to be where these lines intercepted the actual trace.

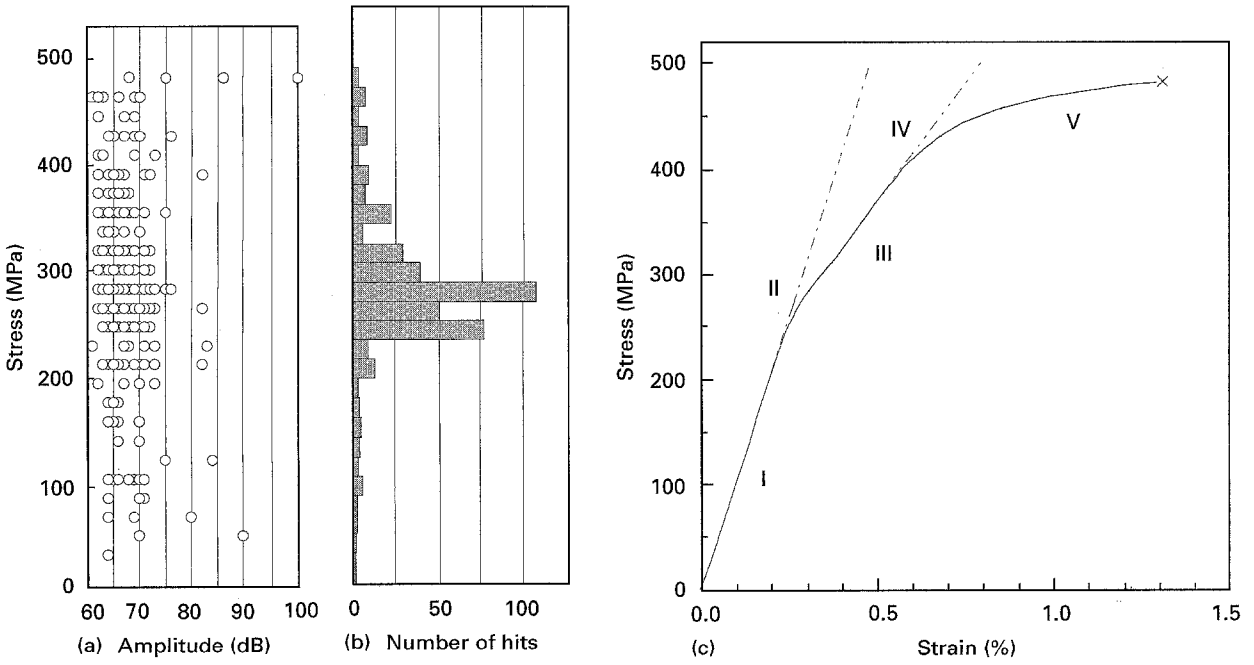

Figure 1 Typical plots from a transverse tensile test performed on Ti–6–4/ SM1140 + , showing the response to increasing specimen stress of (a) the amplitude of AE events, (b) the number of AE events, and (c) the strain in the specimen: (—) actual trace, (×) failure, (— - —) linear extension 1, (— - - —) linear extension 2.

TABLE I Transverse tensile properties measured from stress versus strain traces such as Fig. 1

Property	Position on stress versus strain trace
Elastic modulus of composite	Gradient of linear region I
Stress and strain at the onset of interface failure	Start of curved region II
Stress and strain at the end of interface failure	End of curved region II
Elastic modulus of matrix after debonding	Gradient of second linear region III
Matrix yield stress and strain	Start of curved region IV
Final failure stress and strain	End of region V

3.2. Effect of strain rate on tensile properties

This batch of tests was performed on specimens cut from plate II of the Ti–6–4/SM1140 + composite, and involved the measurement of tensile properties at displacement rates of 1, 10, 100, 1000 and 10 000 μm min^{-1}. The properties measured from each test are set out in Table II and plotted in Fig. 2. It is apparent that there is a reasonable level of consistency between values measured at the same displacement rate, and any trends observed in the data may therefore be accepted with some confidence.

Considering first the significant stress levels measured during testing (Fig. 2a), there is a clear increase in interface debond, matrix yield and final failure stresses as the displacement rate is raised from 10 μm min^{-1} to 10 000 μm min^{-1}. This trend is reflected in the values of percentage strain (Table II) at which these events occur, and is reminiscent of the effects of varying the displacement rate on values of yield and failure stress in monolithic alloys. However, the results from tests at the slowest ramp rate used here (1 μm min^{-1}) do not follow this trend, and the debond and yield stresses are similar to those measured at 10 μm min^{-1}.

TABLE II Transverse tensile properties of a Ti–6–4/SM1140 + composite (plate II) measured at different displacement rates

Ramp rate (μm min^{-1})	Interface debonding		Matrix yield		Final failure			Moduli (GPa)	
	Stress (MPa)	Strain (%)	Stress (MPa)	Strain (%)	Stress (MPa)	Strain (%)	Plastic strain	First linear	Second linear
10 000	285–290	0.25–0.25	425	0.56	505	1.49	1.07	119	43.8
1 000	285–290	0.25–0.26	405	0.52	475	1.21	0.80	116	43.9
1 000	285–290	0.25–0.26	395	0.49	480	1.21	0.80	117	45.2
100	265–285	0.24–0.27	385	0.49	460	0.92	0.51	113	44.3
100	255–280	0.23–0.26	385	0.48	450	0.86	0.47	116	45.2
10	245–265	0.22–0.25	350	0.43	395	0.60	0.26	116	45.3
10	240–260	0.21–0.24	340	0.42	415	0.89	0.53	116	44.2
1	240–265	0.22–0.26	355	0.46	440	1.41	1.01	110	45.0
1	260–275	0.24–0.26	345	0.42	460	1.49	1.07	110	45.3

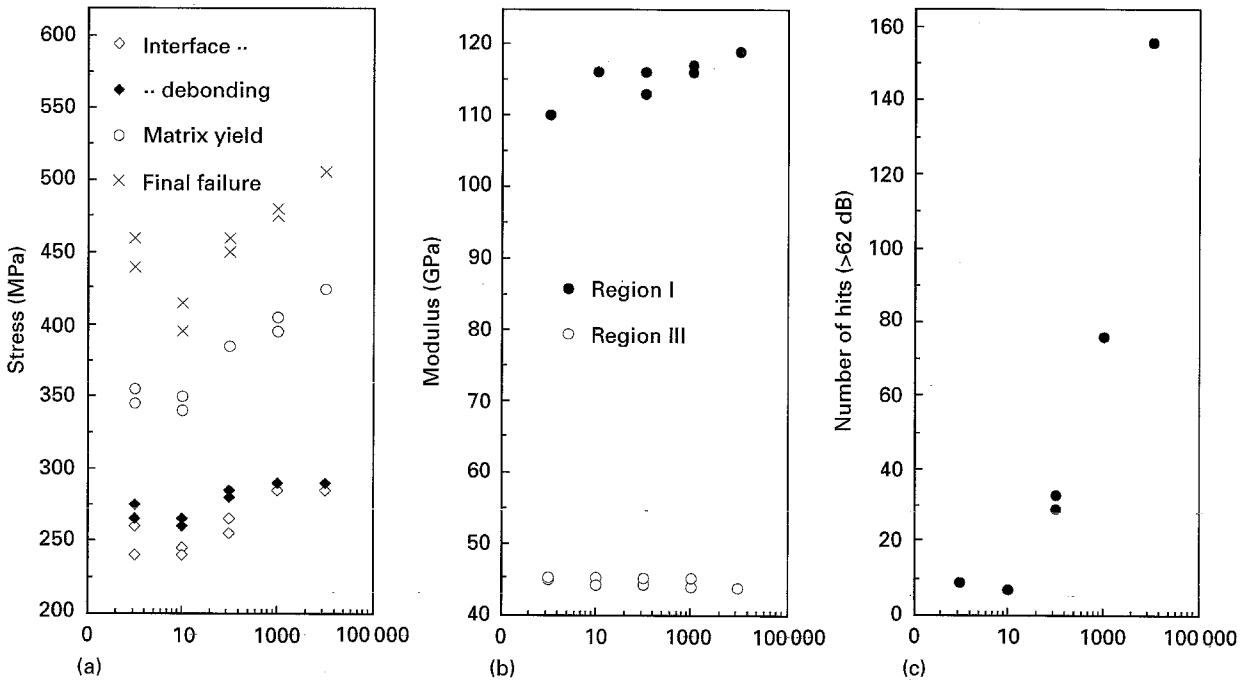

Figure 2 Effect of varying the displacement rate on (a) interface debonding, matrix yield and failure stresses, (b) elastic moduli, and (c) the number of higher amplitude (⩾ 62 dB) acoustic emissions. (a) (◇) start of interface debonding (◆) end of interface debonding, (○) matrix yield, (×) final failure. (b) (●) Region I, (○) Region III.

A comparison of the gradients of the linear regions (I and III) of the stress versus strain trace (shown in Fig. 2b) suggest that these are relatively insensitive to displacement rate. The gradient of region I, which represents the elastic deformation of the whole composite, yields a transverse Young's modulus for plate II of approximately 115 ± 5 GPa. The lowest and highest values are noted for the slowest and fastest displacement rates, respectively, but the modulus remains relatively constant for rates of between 10 and 1000 $\mu m\,min^{-1}$. Linear region III represents the elastic deformation of the matrix ligaments between the debonded fibres, and yields a value for the gradient of 44.6 ± 0.8 GPa. There is an indication that this value decreases slightly as the displacement rate is increased, but otherwise it is relatively constant.

A further interesting observation was that there was a clear effect of the displacement rate on the number of higher amplitude acoustic emissions recorded (see Fig. 2c), in that there were few at low rates ($\leqslant 10\ \mu m\,min^{-1}$) but that the numbers significantly increased as the ramp rate rose to 10 000 $\mu m\,min^{-1}$. (N.B. the AE data shown in Fig. 2c were collected using a less-sensitive sensor than that used to collect the data shown in Figs 1 and 4, and the measured amplitudes are therefore around 10 dB lower.)

Fractographic examination of the rupture surfaces showed no obvious differences in failure mode as a function of displacement rate. The surfaces are fairly flat and consist of thin bands of matrix alloy between a mixture of protruding fibres and empty fibre channels. There was no fibre failure, and the predominant mode of matrix failure was microvoid coalescence (Fig. 3c). In a few cases, however, where the width of the matrix ligament between fibres was small, a more faceted surface was observed (Fig. 3a and b).

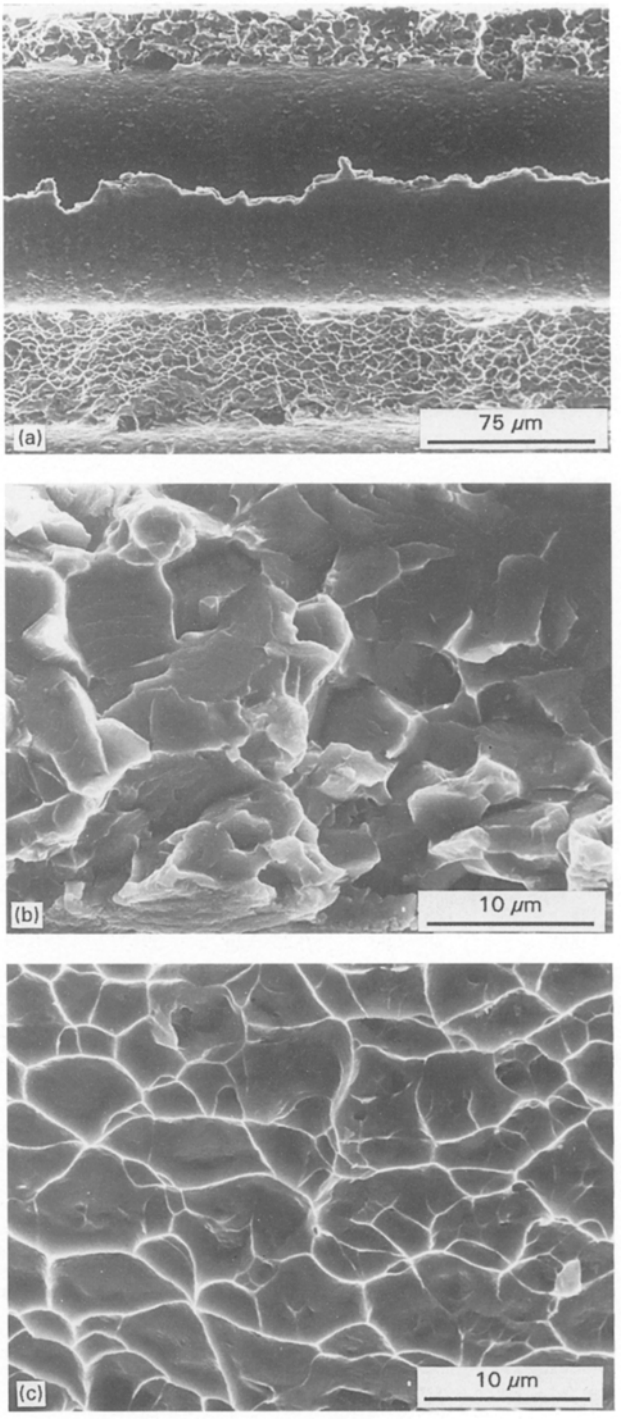

Figure 3 Fractographs of a rupture surface resulting from a monotonic tensile test performed at a displacement rate of 1 $\mu m\,min^{-1}$, showing features from (a) thin and thick, (b) thin, and (c) thick matrix ligaments between fibres.

3.3. Effect of pre-damage on tensile properties

The investigation into the effects of pre-damage was performed on testpieces of Ti–6–4/SM1140 + cut from plate I. Initial work concentrated on the properties of specimens which had been pre-stressed to a value of 200 MPa, either by a simple ramp or a number of fatigue cycles, and the results are displayed in Table III. This stress lies within the linear elastic region I, and is therefore below that at which failure of the fibre/matrix interfaces occurs. It was therefore not surprising that neither a single ramp nor 100 000 fatigue cycles (approximately 60% of the total life) up to a stress of 200 MPa had any significant effect on the transverse stress versus strain response observed in subsequent tensile tests.

A further test was performed on a specimen which had been pre-stressed using a single ramp to 350 MPa, which is within region III of the stress versus strain curve. This ramp should have led to full debonding of the fibre/matrix interfaces within the composite, and indeed was found to have had a dramatic effect on the subsequent tensile properties. The stress versus strain curves produced during pre-stressing, unloading and the subsequent tensile test are shown in Fig. 4, which also plots the amplitude of acoustic emissions recorded during pre-stressing and testing to failure as a function of stress on the specimen. The pre-stressing plot is typical of that seen for this composite (see Fig. 1), but on unloading there is a non-linear trace which does not return to the origin, showing that loading up to 350 MPa puts a small permanent strain into the matrix. On re-loading, the trace is close to, but just above that resulting from unloading, and again shows no significant linear region. Once the stress reaches the level of pre-stress, however, the curve rejoins the path that would result from a simple

TABLE III Transverse tensile properties of a Ti–6–4/SM1140 + composite (plate I) measured from as-cut and pre-stressed testpieces

Testpiece history	Interface debonding		Matrix yield		Final failure			Moduli (GPa)	
	Stress (MPa)	Strain (%)	Stress (MPa)	Strain (%)	Stress (MPa)	Strain (%)	Plastic strain	First linear	Second linear
None	250–270	0.24–0.27	400	0.56	485	1.30	0.85	107	44.6
None	245–265	0.24–0.27	395	0.55	480	1.11	0.64	103	45.9
Pre-stress	230–265	0.22–0.27	395	0.57	495	1.65	1.18	105	43.2
Pre-fatigue	255–275	0.25–0.27	395	0.54	495	1.47	1.00	106	45.1

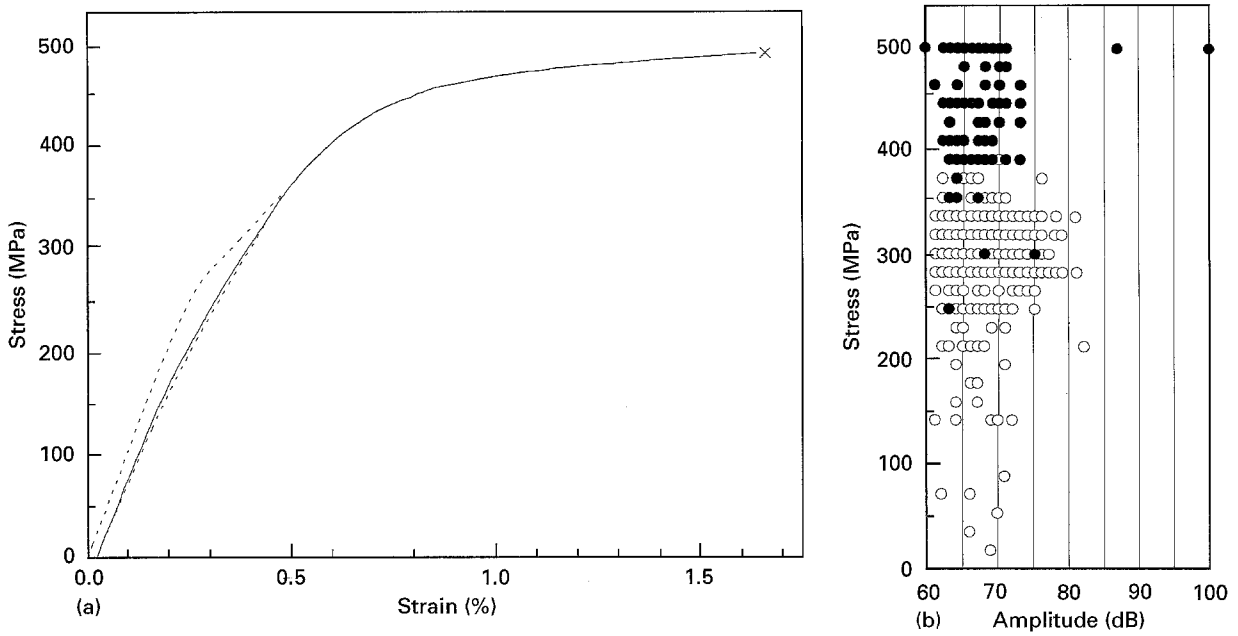

Figure 4 Plots from a transverse tensile test, showing (a) the stress versus strain response during (- - -) pre-stressing, unloading and (—) the subsequent tensile test, and (b) the amplitude of AE events recorded during (○) pre-stressing and (●) testing to failure. (×) Failure.

continuous tensile test (compare with Fig. 1). The acoustic emissions recorded during pre-stressing were typical for this type of test, but on re-loading there were almost no emissions at stresses up to the pre-stress level. At higher stresses, however, the emission characteristics were similar to those observed previously for a simple monotonic ramp to failure.

3.4. *S–N* fatigue properties

The results of the cyclic loading tests performed on plane-sided specimens cut from plate II of the Ti–6–4/SM1140 + composite are shown in Fig. 5, in the form of a maximum applied stress versus cycles to failure plot. An initial plot of all the data showed a large degree of scatter, but it was noted that there were two distinct groups of specimens, divisible by a variation in plate thickness. The data from specimens of each width (1.33 and 1.35 mm) are therefore displayed separately in Fig. 5, revealing that the fatigue lives of the thicker specimens were up to six times longer than those measured for the thinner samples.

Metallographic examination of a sample from each group revealed no significant variation in the fibre volume fraction (≈33%) within plate II, but there was

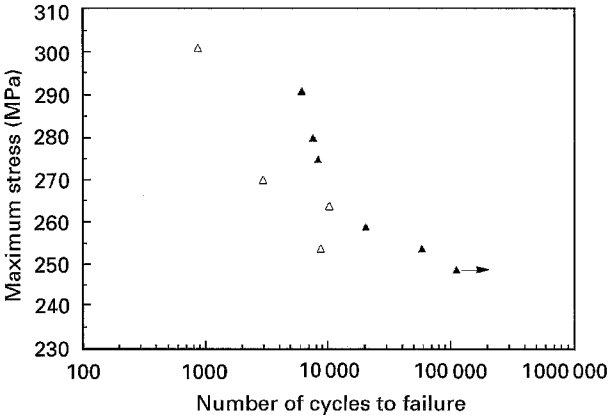

Figure 5 Plot showing the number of cycles to failure as a function of maximum stress for low-cycle fatigue tests performed on Ti–6–4/SM1140 +. (▲) 1.35 mm width, (△) 1.33 mm width.

a noticeable difference in the uniformity of the fibre arrangement. This is demonstrated by the histograms in Fig. 6 which show that, within a fibre mat, 73% of the fibre edge-to-edge spacings are within 12 μm of the average (≈38 μm) for the wider (1.35 mm) specimen, compared to only 51% for the thinner (1.33 mm) specimen. In addition, in the thinner specimen there were

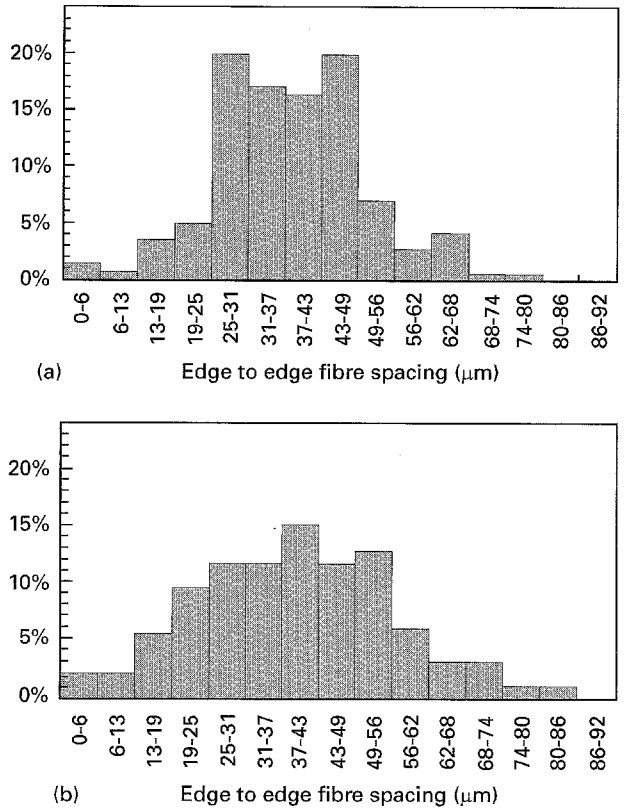

Figure 6 Histograms showing the distribution of fibre edge-to-edge spacings within a fibre mat for (a) a 1.35 mm wide sample, and (b) a 1.33 mm wide specimen.

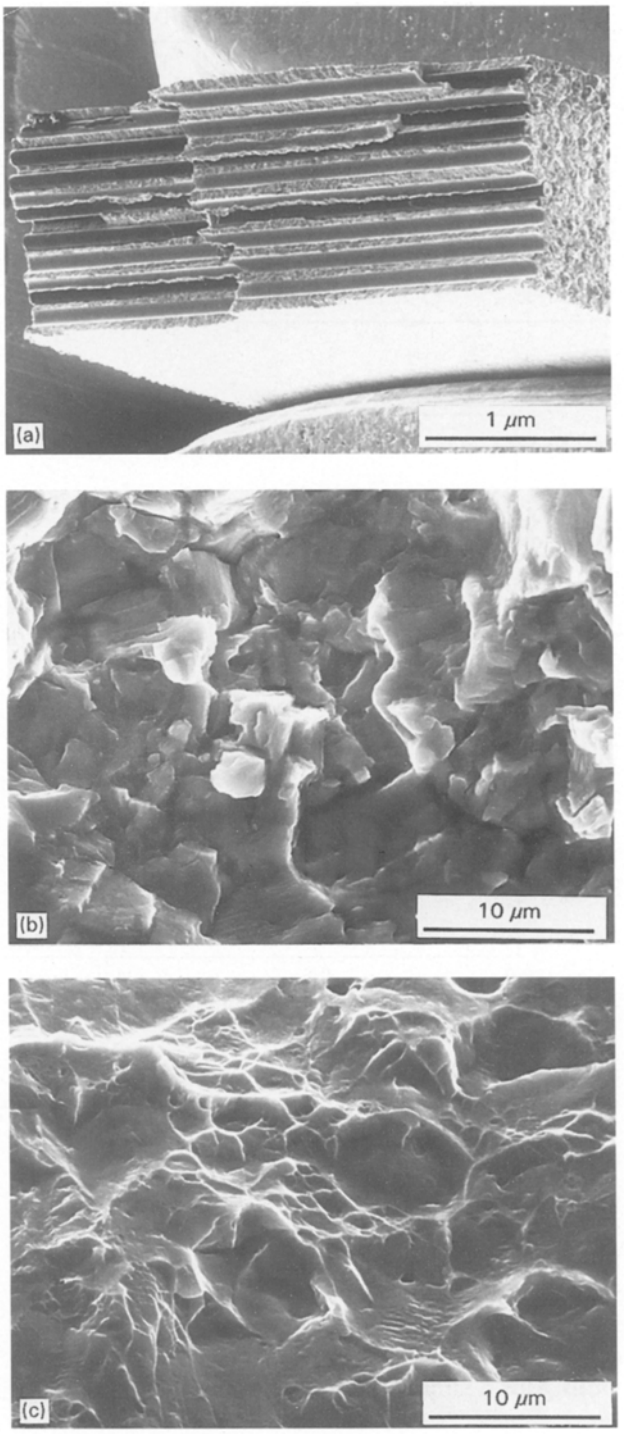

Figure 7 Fractographs of the rupture surface from a sample fatigued with a maximum stress of 291 MPa, showing (a) cracking on different planes, (b) faceted fatigue markings, and (c) microvoid coalescence/shear during final failure.

many more fibres separated by less than 13 μm of matrix in comparison with the thicker specimen (5% compared with 2%). These histograms were each produced from approximately 150 measurements.

The data shown in Fig. 5 from the 1.35 mm specimens suggest that there are two distinct linear regions to the maximum stress versus number of cycles to failure relationship, with the transition being at a stress of around 260–265 MPa. Unfortunately, the acoustic emission data collected during fatigue testing were largely inconclusive. They did, however, show that the majority of the significant events (> 60 dB) occurred during the first fatigue cycle, and more generally that events were occurring throughout the trapezoidal cycle (apart from during the dwell at minimum load), i.e. during loading, the dwell at maximum load and unloading.

Fractographic examination of the fatigue rupture surfaces revealed that fatigue/final failure occurred along a small number of adjacent planes, creating a stepped fracture surface (Fig. 7a). The fatigued region, which had a faceted appearance (Fig. 7b), was quite different from that resulting from final failure, where evidence of both shearing and microvoid coalescence could be observed (Fig. 7c). There were, however, no obvious differences between the rupture surfaces produced at different maximum stress levels.

The point of initiation of the fatigue crack was difficult to discern, as the presence of fibres obliterated any obvious features which might have led back to that point. Indeed, it is probable that the fibre/matrix interfaces offer many potential initiation sites away from the specimen edge, and that no single dominant initiation site exists. In some regions of the fatigue surface striations can be seen (Fig. 8), in this case suggesting that the crack grew down from one fibre to the next, rather than along the matrix ligament. The spacings between the striations shown in Fig. 8 range from 0.3–0.7 μm, with the average spacing being ≈ 0.55 μm or 5.5×10^{-4} mm.

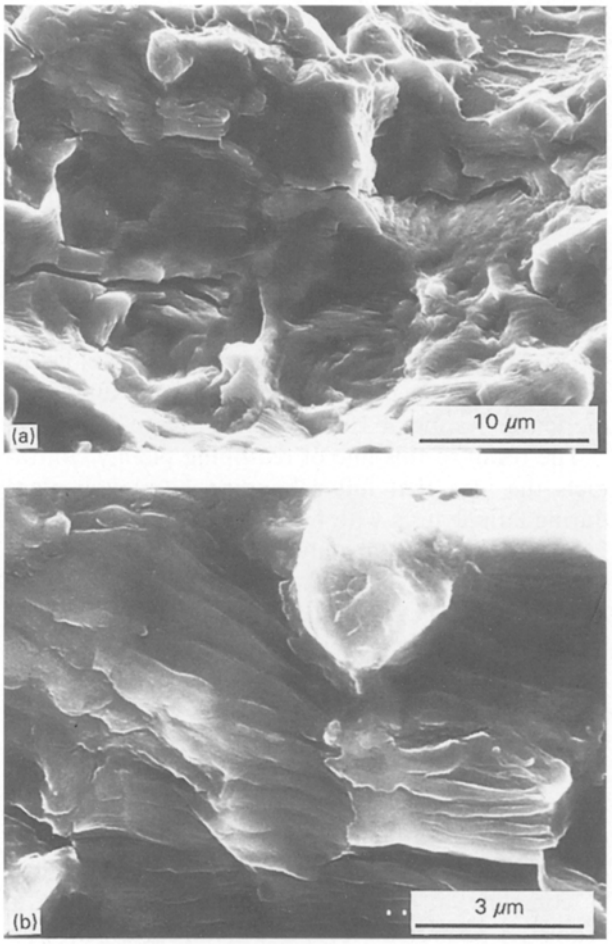

Figure 8 Fractographs showing fatigue striations on the rupture surface of a sample fatigued with a maximum stress of 254 MPa.

4. Discussion

4.1. Tensile properties

The form of the stress versus strain relationship shown in Fig. 1 remained consistent for all of the tensile tests performed during this work, and is identical in character to that recorded by other researchers working on titanium matrix composite systems. Majumdar and Newaz [10] noted the excellent reproducibility of a similar stress versus strain response in a Ti–15–3/SCS-6 composite, and identified the same significant features which were noted here for Ti–6–4/SM1140 + .

The initial linear region (I) undoubtedly represents the elastic deformation of the composite, and on unloading during this region, strain is fully recoverable. Unloading from the second linear region (III), however, reveals a significant reduction in the gradient of the unloading and reloading curves and that a small amount of permanent plastic strain ($\approx 0.025\%$) has been put into the specimen (Fig. 4). Majumdar and Newaz [10] observed near identical behaviour on unloading and, using specimen compliance and Poisson's ratio measurements, they determined that loading beyond the first bend in the curve (region II) resulted in significant damage and a limited amount of plasticity. The large number of acoustic emissions recorded during region II in the current work supports such findings. Previous research [11] has demonstrated that, under transverse loading, events with amplitudes of between 60 and 80 dB (such as those recorded here in Figs 1 and 4) result from damage to the fibre/matrix interface, leading to full debonding. Once pre-stressing above the interface debond stress has occurred, the composite behaves like a monolithic material containing rows of constrained "holes". This leads to non-homogeneous straining of the matrix along the length of the specimen, resulting in the non-linear nature of the unloading and reloading curves in Fig. 4.

In contrast, when unloading from a higher stress beyond the second bend in the trace (region IV), Majumdar and Newaz [10] noted that there was a much greater influence of plasticity than damage. This confirms that region IV represents yielding of the matrix rather than an interface-related phenomenon. Indeed, the *bulk* stress at which the curve deviates from the linear (at $100\ \mu m\ min^{-1}$) is around 380–400 MPa, yielding a realistic *net* ligament yield stress for Ti–6–4 of 930–980 MPa. Final failure of the specimen then proceeds through plastic straining and necking of the matrix ligaments during region V, and a similar calculation yields a *net* failure stress for the Ti–6–4 ligaments of around 1100–1170 MPa. It was to be expected that the resulting fracture surfaces would be predominantly made up of features showing microvoid coalescence (Fig. 3c), but the reason for the more faceted appearance of the surface where the matrix ligament was thin (Fig. 3b) is not obvious, and necessitates further study.

The effect on tensile properties of varying the displacement rate is clear from Fig. 2a, in that the debond, yield and failure stresses increase as the ramp rate rises from $10\ \mu m\ min^{-1}$ to $10\,000\ \mu m\ min^{-1}$. Such an observation concerning matrix yield and failure is not surprising in that it is compatible with trends observed in monolithic alloys. The reason for the effect of displacement rate on the debonding stress is less well established, but a possible explanation was provided by the acoustic emissions data (Fig. 2c). These results show an effect of displacement rate on the number of higher amplitude emissions, in that there were many more recorded at $10\,000\ \mu m\ min^{-1}$ than at very low rates ($\leqslant 10\ \mu m\ min^{-1}$). This does not mean that a greater number of interface failures occur during faster tests, as it is likely that many events resulting from debonding are too small to be detected by the equipment as it was set up for this work. Rather, it simply suggests that increasing the displacement rate results in a greater number of *high amplitude* events.

It may be conjectured that interface failure is a gradual process at a slow displacement rate, and occurs through a large number of small events (not detected here). At a high displacement rate, however, a more rapid straining of the interface may not allow this. The rapid increase in the stress could extend elastic behaviour beyond the stress level at which interfacial failure begins at low ramp rates, resulting in the instantaneous failure of relatively large lengths of interface at a higher stress. The failure of larger lengths of interface could be the source of the greater number of higher amplitude acoustic emissions recorded at faster ramp rates, and such a scenario would explain

TABLE IV Comparison between the transverse tensile properties of specimens cut from different plates of the Ti–6–4/SM1140 + composite

Property		Plate I	Plate II
Elastic modulus of composite	(GPa)	105 ± 2	115 ± 2
Interface failure stress range	(MPa)	230–275	255–285
Elastic modulus of matrix	(GPa)	44.6 ± 1.4	44.7 ± 0.5
Matrix yield stress	(MPa)	395	385
Final failure stress	(MPa)	490 ± 10	455 ± 5
Fibre volume fraction		31%	33%

both the increase in interface debond stress and the narrow stress band over which debonding occurs at higher displacement rates (see Fig. 2a and Table II).

The effect of displacement rate on transverse properties has implications when using tensile data to explain the results from fatigue tests, where high displacement rates are used, and this will be discussed further in the next section. The trend does not extend to very low ramp rates, however, and it would seem that any effect of reducing the displacement rate "saturates" at around 10 $\mu m\,min^{-1}$, and that any further slowing makes no significant difference in terms of the ability of the composite to deform in response to the stress imposed upon it.

A final observation of interest is the difference between the properties measured for the two plates used in this work (compare Tables II and III), and the results from tests conducted at 100 $\mu m\,min^{-1}$ are compared in Table IV. This variation in properties is almost certainly a result of the difference in the fibre volume fraction of the two plates (33% in plate II compared to 31% in plate I). A higher volume fraction of reinforcement would be expected to result in better properties prior to interface failure, and inferior properties afterwards (when there is less load-bearing matrix), and this is indeed found to be the case. Specimens cut from plate II have a higher elastic modulus and undergo interfacial failure at a higher stress. Once this has occurred, however, they yield and fail at a lower stress than for specimens cut from plate I.

4.2. Low-cycle fatigue

The low cycle fatigue lives measured in transverse specimens of Ti–6–4/SM1140 + are shown in Fig. 5. The narrow range of maximum stresses used during this work (250–300 MPa) was chosen in order to investigate the differences between the fatigue lives of specimens where interfacial failure had either partially or fully occurred. The most obvious feature is the change in gradient at a maximum stress of around 260–265 MPa. At stresses below this transition there is a strong dependency of fatigue life on maximum stress, but this is not so above the transition point. This suggests that there is a significant change in the fatigue process over the lower range of stresses studied here, which is most likely to be connected with progressive interfacial failure. In which case, the relative insensitivity of fatigue lives to maximum stresses above the transition ($\geqslant$ 265 MPa) would indicate that full interface debonding has taken place in each of these specimens, and that the modest reductions observed in the fatigue lives at higher stresses are entirely due to increased loading of the unreinforced matrix.

In order to relate this observation to the tensile behaviour, the displacement rate during the fatigue cycle must first be calculated. If only the initial 1 s ramps up to maximum load are considered, these occur at displacement rates ranging from 18 000–23 000 $\mu m\,min^{-1}$. It might therefore be expected that interface failure and debonding during fatigue should not occur at maximum stresses below 285–290 MPa, the debond stress range measured during tensile testing at 10 000 $\mu m\,min^{-1}$ (see Table II).

The result of this line of reasoning plainly contradicts the idea that full debonding has taken place during fatigue tests with maximum stresses as low as 265 MPa, but thus far only the first part of the trapezoidal cycle has been considered. The increase in debonding stress at higher displacement rates is thought to reflect the lack of time available for small-scale time-dependent damage of the interface. During a trapezoidal fatigue cycle, however, there is a dwell period at maximum load, which will allow some time during each cycle for such processes to occur. It could be argued that, over a period of time, the repeated dwells during fatigue create similar conditions to a slower displacement rate test, where interface failure is complete at stresses of around 260–265 MPa (Table II). Such stress levels are in full agreement with the transition maximum stress measured from Fig. 5, and the acoustic emission data collected during testing lend support to this idea. Hits recorded during dwells at maximum load occur throughout the whole of the 1 s period, suggesting that significant interfacial failures do take place during this part of the fatigue cycle.

The other main point of interest from the fatigue results presented in Fig. 5 was the variation in behaviour with plate thickness. The histograms in Fig. 6 demonstrate that the fibre arrangement was more regular in the thicker (1.35 mm) part of plate II than in the thinner area, and this is the most likely explanation for the variations in fatigue life, as no other obvious differences between the two groups of samples were observed. However, the exact reason why irregular fibre spacings should have such a dramatic effect on fatigue lives is unclear. A possible reason is that there were significantly more instances of fibres which either touched or were very close together in the thinner specimens (Fig. 6), which had shorter fatigue lives (Fig. 5), and it may be that touching fibres act as larger defects in the composite. Whatever the explanation, it is clear that uniformity of fibre spacing is a critical requirement for producing composites with good and reproducible transverse properties under fatigue loading.

5. Conclusions

1. The transverse stress versus strain response of a Ti–6–4/SM1140 + composite demonstrates that each specimen undergoes five significant processes up to the point of specimen failure, which are (I) elastic

deformation of the composite, (II) fibre/matrix interface debonding, (III) elastic deformation of matrix ligaments, (IV) yield of matrix ligaments, and (V) gross plastic deformation of the matrix.

2. Exposure to a stress above the interface debond stress results in the composite behaving like a non-homogeneous monolithic titanium specimen which contains a series of constrained "holes", and thus undergoes non-linear straining on reloading.

3. There is a clear effect of displacement rate on transverse tensile properties. Increasing the ramp rate from $10\,\mu m\,min^{-1}$ to $10000\,\mu m\,min^{-1}$ results in a progressive rise in the stresses at which interfacial failure, matrix yield and final failure occur.

4. A small increase in the volume fraction of fibres (from 31% to 33%) leads to a higher elastic modulus and interface debond stress, but inferior properties after interfacial failure.

5. Low-cycle fatigue life is strongly influenced by the occurrence of interfacial failure, which fully occurred at stresses above 260–265 MPa in Ti–6–4/SM1140 + when using a 0.25 Hz *trapezoidal* waveform.

6. Uniformity of fibre spacing may play a critical role in determining the transverse fatigue life of Ti–6–4/SM1140 + .

Acknowledgements

The authors are grateful to Professor M. H. Loretto for provision of laboratory facilities at the I.R.C. in Materials for High Performance Applications and to Rolls Royce for their financial support, advice and provision of material. Helpful discussions have been held with many colleagues, but particular thanks are due to Mike Hartley at Rolls Royce, Derby, and to the members of the Fatigue and Fracture Group at Birmingham.

References

1. S. M. JENG, J.-M. YANG and C. J. YANG, *Mater. Sci. Eng.* **A138** (1991) 169.
2. S. M. JENG, P. ALASSOEUR, J.-M. YANG and S. AKSOY, *ibid.* **A148** (1991) 67.
3. D. WALLS, G. BAO and F. ZOK, *Scripta Metall. Mater.* **25** (1991) 911.
4. P. J. COTTERILL and P. BOWEN, *Composites* **24** (1993) 214.
5. A. R. IBBOTSON, C. J. BEEVERS and P. BOWEN, *Scripta Metall. Mater.* **25** (1991) 1781.
6. K. M. FOX, M. STRANGWOOD and P. BOWEN, *Composites* **25** (1994) 684.
7. C. BARNEY, C. J. BEEVERS and P. BOWEN, *ibid.* **24** (1993) 229.
8. D. L. DAVIDSON, *Metall. Trans.* **23A** (1992) 865.
9. N. WANG, D. C. CARDONA and P. BOWEN, *Int. J. Fract.* (1996) in press.
10. B. S. MAJUMDAR and G. M. NEWAZ, *Philos. Mag.* **66** (1992) 187.
11. J. G. BACKUCKAS, W. H. PROSSER and W. S. JOHNSON, *J. Compos. Mater.* **28** (1994) 305.

Received 16 February
and accepted 18 March 1996